American Mineralogist, Volume 93, pages 217–227, 2008

Pressure dependence of the hydrogen-bond geometry in topaz-OD from neutron powder diffraction

K. KOMATSU,[1,2,*] H. KAGI,[2] W.G. MARSHALL,[3] T. KURIBAYASHI,[1] J.B. PARISE,[4] AND Y. KUDOH[1]

[1]Institute of Mineralogy, Petrology and Economic Geology, Graduate School of Science, Tohoku University, Sendai 980-8578, Japan
[2]Geochemical Laboratory, Graduate School of Science, The University of Tokyo, Tokyo 113-0033, Japan
[3]ISIS Neutron Facility, Rutherford Appleton Laboratory, Harwell Science and Innovation Campus, Didcot, Oxon, OX11 0QX, U.K.
[4]Mineral Physics Institute, Department of Geosciences, State University of New York, Stony Brook, New York 11794-2100, U.S.A.

ABSTRACT

The crystal structure of deuterated topaz [topaz-OD; $Al_2SiO_4(OD)_2$], synthesized at 10 GPa and 800 °C, has been determined using neutron powder diffraction at pressures up to 7.5 GPa. The linear axial compressibilities obtained from regressions of the lattice constants vs. pressure are $\beta_a = 1.87(1) \times 10^{-3}$ GPa^{-1}, $\beta_b = 1.71(1) \times 10^{-3}$ GPa^{-1}, and $\beta_c = 2.73(1) \times 10^{-3}$ GPa^{-1}. The occupancy of the D1 site was found to be greater than that of D2, as shown independently using neutron diffraction and infrared spectra at ambient conditions. A bifurcated hydrogen bond involving the D1 site, O4-D1···O2 and O4-D1···O3, and a trifurcated hydrogen bond involving D2 site, O4-D2···O1, O4-D2···O2, and O4-D2···O4 are proposed for hydrogen-bond donor and acceptor pairs in addition to those reported previously. The observed pressure dependences of the hydrogen-bonding geometry show that these donor and acceptor pairs are classifiable into two types of interaction: (1) those that strengthen as a function of pressure (O4-D1···O3, O4-D2···O2, and O4-D2···O4) and (2) those that weaken (O4-D1···O1 and O4-D2···O1). These results also demonstrate that the reason for the contrasting behavior of the ν(OH) between F-rich natural topaz and topaz-OH are both the cooperative effect, O4-D2···O4-D1···O3, and the increasing Al-O4 distance.

Keywords: Topaz-OD, hydrogen bond, neutron powder diffraction, high pressure

INTRODUCTION

Hydrogen bonding is a donor-acceptor interaction involving hydrogen atoms in the moiety *X*-H···*Y*. The donor *X*-H covalent bond, which is such as to withdraw electrons and leave the proton partially unshielded, interacts with the acceptor anion *Y*, which must have lone-pair electrons or polarizable π electrons (Jeffrey 1997). The strength of hydrogen bonds is governed by both the donor strength and the acceptor capability, which can be characterized thermodynamically or from theoretically determined hydrogen bond energies (Lutz 2003). However, the hydrogen bond energies are not always capable of being determined by experimental methods. For hydroxides, the details of hydrogen bond geometry, such as O···O distances, along with OH stretching frequencies, and ^{1}H NMR chemical shifts have been used to evaluate the strength of the hydrogen bonding interaction (e.g., Emsley 1980). These experimentally determinable values correlate with each other (e.g., Nakamoto et al. 1955; Novak 1974; Mikenda 1986; Libowitzky 1999; Eckert et al. 1988; Xue and Kanzaki 2004).

Although the correlations between spectroscopic data, geometry, and strength of hydrogen bonds look simple, the physical interpretation of these correlations are complicated by the different sensitivities of the methods and their respective observational time-scales, which effectively provide different descriptions for the hydrogen bond in question. For instance, H···*Y* distances and O-H···*Y* angles may be used as a measure of the strength of the donor-acceptor interaction. On the other hand, the O-H distance and OH stretching frequency reflect the whole potential field surrounding the hydrogen atom. In the case of bent, bifurcated, or trifurcated hydrogen bond interactions, the differences between the conclusions drawn from geometric and spectroscopic observations may become obvious. To further complicate matters, many of the correlations relating hydrogen bond strength to geometric and spectroscopic observables are derived from data measured at ambient conditions. Such correlations are then often used to interpret results obtained under non-ambient conditions. In this case, it is important to specify the limits of validity of such correlations and to know which factors affect to the deviation.

At ambient conditions, an empirical relationship showing a decrease in OH stretching frequency [ν(OH)] with decreasing

* Present address: Centre for Science at Extreme Conditions, The University of Edinburgh, Erskine Williamson Building, Mayfield Road, Edinburgh EH9 3JZ, U.K. E-mail: kom@eqchem.s.u-tokyo.ac.jp

O···O distance [d(O···O)] in the hydrogen bond (O-H···O) was established by Nakamoto et al. (1955) and subsequently refined by Novak (1974), Mikenda (1986), and Libowitzky (1999). Thus, the decreasing d(O···O) has long been believed to be responsible for frequency downshifts. The d(O···O) is much more readily determined using X-ray techniques than d(O-H), d(H···O), and the O-H···O angle as the latter require accurate hydrogen atom positions. In fact, under ambient conditions decreasing d(O···O) generally corresponds to a decrease in ν(OH). However, although ν(OH) is also expected to decrease with increasing pressure because of the decreasing d(O···O), the particulars of the hydrogen bond geometry associated with the position of the hydrogen atom can alter this simple picture.

Hofmeister et al. (1999) showed that ν(OH) increases linearly with pressure for several phases and that linear fits for several mineral groups to the plots of $d\nu/dP$ against ν_{i0}, the value of ν(OH) at ambient pressure, converge at $d\nu/dP = 0.55$ cm^{-1}/GPa and $\nu_{i0} = 3625$ cm^{-1}. That is to say, in the cases when ν_{i0} was greater than 3625 cm^{-1}, ν(OH) increased with pressure even if d(O···O) decreased. Several authors have argued that the hydrogen bond angle influences distance-frequency correlations (e.g., Hofmeister et al. 1999; Kagi et al. 2003). Lutz and co-workers (e.g., Lutz 1988, 2003; Beckenkamp and Lutz 1992; Lutz et al. 1994) have pursued this problem. They reviewed the relationship between the structure and strength of hydrogen bonds in detail, and suggested that the donor strengths and acceptor capabilities that govern the strength of hydrogen bonds are modified by additional phenomena like the synergetic, the cooperative, and the anti-cooperative or competitive effects (see details in Lutz 2003). However, the relationship between ν(OH), hydrogen bond geometry and the strength of hydrogen bond under pressure remains unclear. Apart from the critical factors mentioned above, partial site occupancy, hydrogen-site ordering, and the pressure dependence of these factors can also affect the strength of hydrogen bonding. The relative significance of these factors may be investigated from high-pressure crystallographic studies of the mineral topaz.

Topaz [$Al_2SiO_4(OH,F)_2$] is a well-known accessory hydrous mineral with a limited range of solid solution [OH/(OH + F) < ca. 30%] occurring in near-surface environments (e.g., Ribbe and Rosenberg 1971). A neutron diffraction study of a single-crystal of topaz (Parise et al. 1980) showed that the shortest distance between two hydrogen sites is only 1.5 Å, which is too short for both positions to be occupied, leading to the suggestion that the limit of OH/F substitution is imposed by the geometry of hydrogen sites. However, Wunder et al. (1993) synthesized the OH end-member of topaz from high-pressure experiments at pressures between 5.5 and 10 GPa and temperatures up to 1000 °C in the Al_2O_3-SiO_2-H_2O system. They designated this pure hydroxyl end-member as "topaz-OH" (synthetic OH analogue of topaz, hereafter referred to as topaz-OH without the quotation marks). Northrup et al. (1994) determined the structure of topaz-OH from single-crystal X-ray diffraction data and showed that hydrogen atoms are distributed over two non-equivalent sites (H1 and H2; see Fig. 1 in Northrup et al. 1994). Both sites lie close to the mirror plane in the *Pbnm* space group. Nevertheless, while H2 gives rise to unreasonably short H2-H2 contacts of about 1.7 Å, the neighboring H1 sites are separated by approximately 2.7 Å. The same study reported that the possibility of long-range ordering of hydrogen sites and the reduction of local symmetry was supported by a measurement of the second harmonic generation. However, no evidence for a deviation from the *Pbnm* space group was found that would indicate long-range ordering.

Since the discovery of topaz-OH both natural topaz and synthesized topaz-OH have been investigated by ab-initio or empirical calculations (Churakov and Wunder 2004; Jackson and Valerio 2004), IR and Raman spectroscopy (Pinheiro et al. 2002; Bradbury and Williams 2003; Komatsu et al. 2005), single-crystal X-ray diffraction (Alberico et al. 2003; Komatsu et al. 2003; Gatta et al. 2006a), powder neutron diffraction (Chen et al. 2005), and by combinations of these techniques (Gatta et al. 2006b). Recently, we obtained Raman spectra of topaz-OH up to 17.3 GPa and IR spectra of F-rich natural topaz (F-rich topaz) up to 30.4 GPa (Komatsu et al. 2005). The ν(OH) of topaz-OH shifted to lower frequency with increasing pressure while the ν(OH) of F-rich topaz shifted to higher frequency with increasing pressure (Fig. 6 in Komatsu et al. 2005).

Although F-rich topaz and topaz-OH have identical topological configurations for the Al and Si polyhedra, the circumstances of the hydrogen atoms in the two phases are completely different. Therefore, a comparison of pressure dependence of ν(OH) and crystal structures of F-rich topaz and topaz-OH will help in understanding how hydrogen bond geometry influences the variation of ν(OH) with pressure. For this study, we investigated the crystal structure of deuterated topaz using the time-of-flight neutron powder diffraction technique.

Experimental methods

Sample synthesis

A polycrystalline sample of topaz-OD was synthesized for the neutron diffraction measurements to avoid the high-background scattering that would result from the large incoherent neutron scattering cross section of hydrogen. The starting material for the high-pressure synthesis of topaz-OD was a 2:1 powder mixture of synthetic deuterated gibbsite [$Al(OD)_3$] and SiO_2 in excess D_2O. The deuterated bayerite was synthesized by precipitation from $NaAlO_2/D_2O$ solution held at 80 °C for 3 days. The $NaAlO_2$ was dried at 900 °C for 12 h before dissolution. The product was confirmed as pure bayerite using X-ray powder diffraction. These starting materials were loaded into a welded platinum capsule, which was then placed into a ZrO_2 pressure transmitting medium with a graphite resistance furnace for synthesis in a Kawai-type high-pressure apparatus driven by a pair of guide blocks in a uniaxial 2000 ton press (ERI-2000) installed at the Earthquake Research Institute, University of Tokyo. Eight tungsten carbide (WC) cubic anvils having 8-mm truncation edge lengths were used. The reaction mixture was then subjected to 10 GPa at 800 °C for 2 h. The recovered samples from several synthesis runs were confirmed as topaz-OD using X-ray powder diffraction (MiniFlex; Rigaku Corp.).

Neutron diffraction

Ambient pressure neutron powder diffraction data were collected using the POLARIS diffractometer located at the ISIS facility of Rutherford Appleton Laboratory in the U.K. Ambient and high pressure neutron data were collected using the PEARL/HiPr diffractometer located at the same facility. Different topaz-OD samples were used for the PEARL and POLARIS experiments. Backgrounds higher than expected were observed in the raw data collected at POLARIS that suggested some hydrogen contamination of this sample. This supposition was confirmed in subsequent Rietveld structure refinements of the POLARIS diffraction data. Lower neutron backgrounds, suggestive of much lower hydrogen-contamination, were found for the sample used in the PEARL experiment. Refinements confirmed that the hydrogen sites were mostly occupied by deuterium. Thus, hydrogen atoms were not included in the structure model used for refinement of the PEARL diffraction patterns. Hereafter, the samples studied on POLARIS and PEARL will

be designated by topaz-(OD, OH) and topaz-OD, respectively.

A sample of topaz-(OD,OH) (40 mg), the product of two high-pressure syntheses, was loaded into a SiO_2 glass tube to obtain the neutron powder diffraction patterns at ambient pressure on the POLARIS diffractometer, which has three detector banks centered at $2\theta = 35°$, 90°, 145° covering the *d*-spacing range of 0.36–4.71 Å. For the measurements on PEARL/HiPr a 110 mg topaz-OD sample, the result of four high-pressure synthesis runs, was initially loaded into a thin-walled 5 mm diameter vanadium can to collect ambient pressure diffraction data. This sample was subsequently studied at high pressure using a Paris-Edinburgh (P-E) high-pressure press (Besson et al. 1992) on the same diffractometer. Here it was found that the volume of sample was insufficient to fill completely the standard null-scattering TiZr capsule gasket (Marshall and Francis 2002). The sample was, therefore, mixed with sufficient powdered silica-glass wool to fill the capsule gasket and the mixture was moistened with a few drops of 4:1 deuterated methanol-ethanol pressure transmitting medium. Pressure was applied to the sample through the application of the load to the opposed single toroid WC/Ni-binder anvils using the in situ hydraulic ram of the P-E press. The hydraulic pressure within the ram was monitored and varied by means of a computer-controlled pressure system operating in conjunction with the neutron data acquisition system. High-pressure diffraction patterns were obtained using the large detector bank on PEARL/HiPr centered at $2\theta = 90°$ which were corrected for the effects of neutron attenuation of the incident and scattered neutron beams by the anvil, gasket and shielding materials. During this experiment, patterns were collected for applied cell loads of 7, 15, 25, 38, 46, 58, and 70 tons. The corresponding sample pressures were 0, 0.7, 1.9, 3.6, 4.7, 6.2, and 7.5 GPa, respectively, which were calculated from the refined unit-cell volume using the state equation of topaz-OH, as measured using powder X-ray diffraction. The equation of of state of topaz-OH was first reported by Grevel et al. (2000) [$K = 142.77(1.47)$ GPa, $K' = 4$] and also by Chen and Lager (2005) [$K = 145(4)$ GPa, $K' = 4$]. Since the bulk modulli are consistent to within 1σ, the generated pressures using their equations have no significant difference. In this study, we used the equation of state reported by Chen and Lager (2005). For the pressure calculations, the refined unit-cell volume at the initial sealing load of 7 tons was used as the reference volume V_o in the equation of state relation, because it is likely that the first several tons of load deformed the gasket and did not apply pressure to the sample. For the same reason, all structural parameters excluding lattice constants at 7 tons were fixed to the refined parameters using the ambient pressure data from the sample loaded in the vanadium can.

All of the crystal structure refinements were conducted using the General Structure Analysis System (GSAS) (Larson and Von Dreele 1994). When necessary, the structural parameters of vanadium (ambient data) or WC and Ni (P-E press) were refined along with those of topaz-OD. In all of the refinements an exponential pseudo-Voigt function (GSAS function type 3) was used as the peak profile function. An 8 and 12 term cosine Fourier series was used to model the background contribution for the ambient pressure and high-pressure patterns, respectively.

The initial structure model for the refinement of the ambient pressure data were taken from Northrup et al. (1994), according to which the H(D) atoms occupy two crystallographically inequivalent sites [H1(D1) and H2(D2)]. In the case of topaz-(OD, OH), therefore, we require a site occupancy (*g*) constraint of the form:

$$g(\mathrm{H1}) + g(\mathrm{H2}) + g(\mathrm{D1}) + g(\mathrm{D2}) = 1.$$

It is noteworthy that no other constraints exist for occupancy of H and D atoms. It is not possible to simply apply such a constraint with GSAS, so we adopted the fictitious-atom technique of Joubert et al. (1998). Three fictitious-atoms D11, D12, and D13, were introduced instead of D1, each constrained to have identical atomic coordinates and isotropic atomic displacement parameter (U_{iso}). By means of the following individual constraints on the parameter shifts (δ = shift),

$$\delta g(\mathrm{H1}) = -\delta g(\mathrm{D11}),$$
$$\delta g(\mathrm{H2}) = -\delta g(\mathrm{D12}), \text{ and}$$
$$\delta g(\mathrm{D2}) = -\delta g(\mathrm{D13}),$$

were set. If the summation of initial parameters for occupancies of H and D atoms is set to 1, the required condition of:

$$g(\mathrm{H1}) + g(\mathrm{H2}) + g(\mathrm{D11}) + g(\mathrm{D12}) + g(\mathrm{D13}) + g(\mathrm{D2}) = g(\mathrm{H1}) + g(\mathrm{H2}) + g(\mathrm{D1}) + g(\mathrm{D2}) = 1$$

is ensured provided the occupancies are assigned appropriate initial values.

The diffraction patterns obtained at high pressures were relatively weak and superimposed upon a relatively complex background because of the small quantity of available sample and the amorphous scattering from silica glass. Therefore, for the high-pressure refinements, the data in the *d*-spacing ranges of $d > 3.50$ Å and $d < 0.55$ Å were excluded due to insufficient signal-to-noise discrimination and severe peak overlap, respectively. Starting structural models for each refinement were taken from the refined structure obtained at the previous pressure. It was found that, without the use of the appropriate soft constraints (restraints), the high-pressure pattern refinements yielded negative U_{iso} of Si and unreasonable Si-O bond lengths, as was also reported by Friedrich et al. (2002). Therefore, the isotropic displacement parameters were constrained according to $U_{iso}(\mathrm{Al}) = U_{iso}(\mathrm{Si})$, $U_{iso}(\mathrm{O1}) = U_{iso}(\mathrm{O2}) = U_{iso}(\mathrm{O3}) = U_{iso}(\mathrm{O4})$, and $U_{iso}(\mathrm{D1}) = U_{iso}(\mathrm{D2})$. The soft constraints for the Si-O bond and the O-D distances were applied based on the corresponding values determined at ambient pressure with uncertainty of 0.03 Å.

Some of the possible refinement parameters are highly correlated and so these were fixed during the refinement of the high-pressure structure models. For example, the atomic displacement parameters, U_{iso}, of some atoms converged to unreasonable values when both low intensities and heavy correlation between the absorption coefficient, the g(D1) and g(D2), and the U_{iso} when the absorption coefficient was refined as variable in least-squares for high-pressure data. Therefore, we fixed the g(D1) and g(D2) to the values at ambient pressure. Yet, it is noteworthy that there is no physical reason why the g(D1) and g(D2) are constant with increasing pressure.

Results and discussion

Axial compressibility

Figure 1 shows the Rietveld refinements of the neutron powder diffraction patterns obtained on POLARIS for topaz-(OD,OH) at ambient pressure. In addition, the refinement profiles for topaz-OD at ambient pressure and at 7.5 GPa are shown in Figures 2a and 2b, respectively. The refined lattice constants, experimental conditions and some refinement reliability factors for topaz-(OD,OH) and topaz-OD are shown respectively in Tables 1 and 2.

Figure 3 shows the pressure dependence of the unit-cell parameters of topaz-OD normalized with respect to those at 7 tons load. Also shown in the figure are corresponding values of F-rich topaz obtained by Gatta et al. (2006a). The values obtained by Komatsu et al. (2003) on the same system are consistent with those reported by Gatta et al. (2006a), and so they are not shown in the figure to avoid a complicated figure. The compression curves of lattice constants are almost linear with pressure, or perhaps slightly nonlinear in the case of *c*-axis. The linear axial compressibilities calculated from least-squares fits are $\beta_a = 1.87(1) \times 10^{-3}$ GPa^{-1}, $\beta_b = 1.71(1) \times 10^{-3}$ GPa^{-1}, and $\beta_c = 2.73(1) \times 10^{-3}$ GPa^{-1}. As can be seen from the figure, these compressibilities differ significantly from those observed for F-rich topaz, for which $\beta_a = 2.02(8) \times 10^{-3}$ GPa^{-1}, $\beta_b = 1.42(5) \times 10^{-3}$ GPa^{-1}, and $\beta_c = 2.25(4) \times 10^{-3}$ GPa^{-1} (Komatsu et al. 2003); $\beta_a = 1.99(1) \times 10^{-3}$ GPa^{-1}, $\beta_b = 1.39(1) \times 10^{-3}$ GPa^{-1}, and $\beta_c = 2.18(1) \times 10^{-3}$ GPa^{-1} (Gatta et al. 2006a). However, the anisotropic behavior of topaz-OD (β_a:β_b:β_c = 1.09:1.00:1.60) was also observed for the F-rich topaz [β_a:β_b:β_c = 1.42:1.00:1.58 (Komatsu et al. 2003); β_a:β_b:β_c = 1.43:1.00:1.57 (Gatta et al. 2006a)]. This anisotropic behavior is explained qualitatively from the polyhedral configuration and the stacking direction of closest packing for the oxygen atoms (Komatsu et al. 2003; Gatta et al. 2006a) and was stated previously in Ribbe and Gibbs (1971) as the explanation of {001} cleavage. This cleavage plane is parallel to the only planes in the structure that can be passed through without breaking Si-O bonds. The most compressible **c** axis is also consistent with the fact that {001} represents the plane of the weakest bonds, because Si-O bonds are stiffer than Al-O bonds. Furthermore, compres-

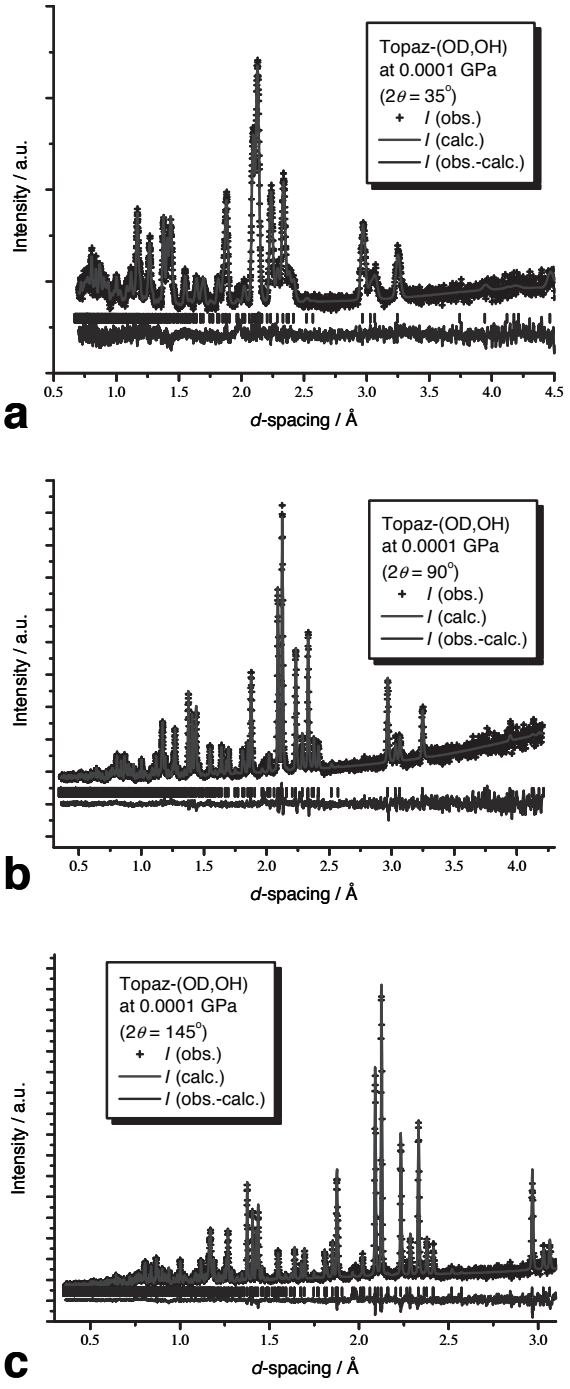

Figure 1. Refinement profiles for topaz-(OD,OH) obtained from the (**a**) 35°, (**b**) 90°, and (**c**) 145° detector banks of POLARIS. The tick marks shown below the profile indicate the position of Bragg reflections for topaz-(OD,OH).

sion along the direction perpendicular to the stacking layer of the closest packing of oxygen, the **b**-axis, was the smallest of the three principal axes. The slight but significant difference of axial compressibilities between F-rich topaz and topaz-OD cannot be explained simply due to complicated compression mechanisms, particularly, in terms of Al octahedron as shown later.

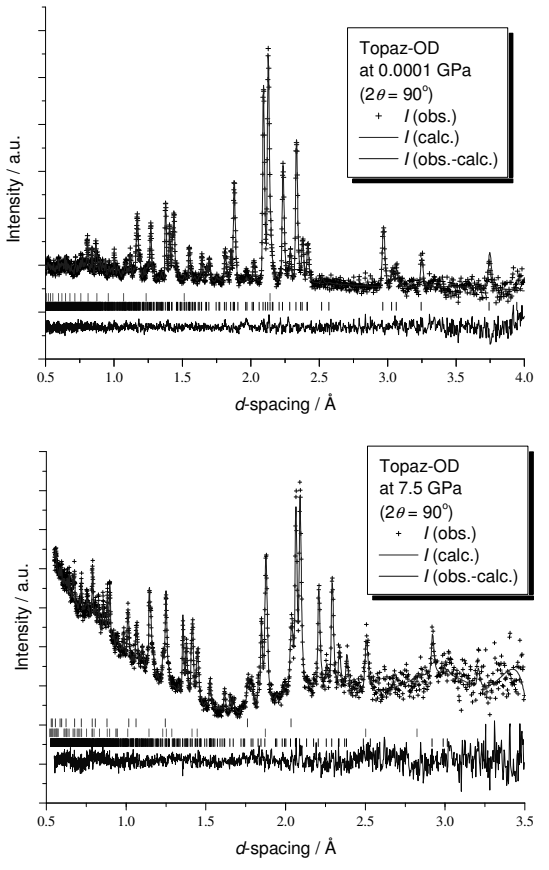

Figure 2. (**a**) Refinement profile for topaz-(OD,OH) at ambient pressure on PEARL/HiPr. The tick marks shown below the profile indicate the position of Bragg reflections for V (upper) and topaz-OD (lower). (**b**) Refinement profile for topaz-OD at 7.5 GPa. The tick marks shown below the profile indicate the position of Bragg reflections for Ni (upper), WC (middle) from the anvil material, and topaz-OD (lower).

Site occupancies of H or D sites

The refined atomic coordinates, isotropic atomic displacement parameters (U_{iso}) and site occupancies (g) for topaz-(OD,OH) at ambient pressure and for topaz-OD at ambient and high pressures are shown in Tables 3 and 4, respectively. Recently, structural details for topaz-OD were obtained from powder neutron diffraction data by Chen et al. (2005), which used the model reported by Northrup et al. (1994) as the starting point for refinement. In both cases the authors assumed site occupancies of hydrogen [g(H1) and g(H2)] or deuterium [g(D1) and g(D2)] fixed to 1/2. However, there is no reason why the [g(H1) + g(D1)] and [g(H2) + g(D2)] should be exactly equal to 1/2 because H1(D1) and H2(D2) in topaz-OH (or -OD) are crystallographically inequivalent sites. Hence, [g(H1) + g(D1)] may in principle be greater than or less than 1/2, and [g(H2) + g(D2)] will be determined from the constraint that the total occupancy of all sites must equal 1. Indeed there is evidence from our neutron diffraction results

and the IR spectra of Wunder et al. (1999) that [g(H1) + g(D1)] is markedly larger than [g(H2) + g(D2)].

The Rietveld refinement of the neutron diffraction data for topaz-(OD, OH) revealed that the site occupancies were g(D1) = 0.432(5), g(D2) = 0.296(5), g(H1) = 0.141(5), and g(H2) = 0.131(5). Hence, the total occupancy of site1 [g(D1) + g(H1)] was 0.57 and that of site2 [g(D2) + g(H2)] was 0.43. For topaz-OD, g(D1) and g(D2) were, respectively, 0.59(2) and 0.41(2).

TABLE 1. Conditions of neutron diffraction measurements and crystallographic data for topaz-(OD,OH)

Name	topaz-(OD,OH)			
Chemical composition	$Al_2SiO_4(OD_{1.45},OH_{0.55})_{\Sigma 2.0}$*			
Z	4			
Load/tons	–			
Pressure (GPa)	0.0001			
Molecular weight, M_r	181.49			
Crystal system	orthorhombic			
Space group	*Pbnm* (no. 62)			
diffractometer	POLARIS at ISIS, RAL			
Specimen condition	powder in quartz-capillary			
2θ of detector bank (°)	35	90	145	total
Lattice constants (Å)				
a	4.72665(5)			
b	8.92817(10)			
c	8.42569(9)			
Unit-cell volume, V_c (Å)	355.567(7)			
Molar volume (calc.), V_m (cm³/mol)	53.53			
Density (calc.), d (g/cm³)	3.39			
d_{min} (Å)	0.7	0.36	0.36	0.36
d_{max} (Å)	4.71	4.37	3.09	4.71
No. data points	3732	4872	4295	12899
No. reflections	687	4809	4484	9980
No. variables	63	63	63	63
R_p†	0.0412	0.0506	0.0468	0.0476
R_{wp}‡	0.0485	0.0386	0.0319	0.0355
R_{F^2}§	0.0732	0.0549	0.0451	0.0592
R_e‖	0.0591	0.0378	0.0231	0.0323
S#	0.82	1.02	1.38	1.1

* The OH/OD ratio was determined from the refined site occupancies.
† $R_p = \Sigma_i|y_i - f_i(\boldsymbol{x})|/\Sigma_i y_i$.
‡ $R_{wp} = [\Sigma_i w_i\{y_i - f_i(\boldsymbol{x})\}^2/\Sigma_i w_i y_i^2]^{1/2}$.
§ $R_{F^2} = \Sigma|F_o^2 - KF_c^2|/\Sigma F_o^2$.
‖ $R_e = [(N-k)/\Sigma_i w_i y_i^2]^{1/2}$.
$S = R_{wp}/R_e = [\Sigma_i w_i\{y_i - f_i(\boldsymbol{x})\}^2/(N-k)]^{1/2}$,
where w_i = statistical weight, y_i = the observed diffraction intensities, $f_i(\boldsymbol{x})$ = the calculated diffraction intensities, F_o = the observed structure factor, F_c = the calculated structure factor, K = a scale factor and the sum extends over all the observed reflections, N = number of data points, k = number of parameters.

The results obtained from the two distinct patterns and samples, obtained from two different instruments, are mutually consistent within experimental error. Although neutron diffraction is the most direct method for demonstrating the non-equality of the site occupancies, the correlation between U_{iso} and the g(D) might be expected to lead to some ambiguity in the crystallographic results obtained. This is emphasized in Figure 4, where the refined U_{iso} and g(D) are plotted, when g(D1) [=1 – g(D2)] was fixed to 0.45–0.70 in the refinement. Figure 4 represents the strong positive correlation between U_{iso} and g. For example, when g(D1) is fixed to 1/2 the U_{iso}(D1) and the U_{iso}(D2) are almost equal because of the correlation effect. Therefore, it might be difficult to say that g(D1) is around 0.6 exclusively from the minimum reduced χ^2. However, it is likely that g(D1) is at least larger than g(D2) because the condition of g(D1) > g(D2) was obtained even when the constraint of U_{iso}(D1) = U_{iso}(D2) was applied. Although the absolute value of site occupancy correlates with displacement parameter, which is not an unexpected result, it appears that the differences in occupancies between sites 1 and 2 persist regardless of the refinement strategy adopted.

A second line of evidence arises from estimations of the site occupancies of H1 and H2 sites from IR spectra in the OH stretching region of powdered topaz-OH reported by Wunder et al. (1999). They showed two strong bands at 3602.1 and 3526.3 cm^{-1}, and a weak band at 3457.0 cm^{-1} (Fig. 4c in Wunder et al. 1999). The absorbance ratio of these three bands was 31:59:10. The two former strong bands might correspond to O-H1 and O-H2 stretching modes, but the latter weak band remains unassigned. Recently, Churakov and Wunder (2004) predicted the existence of four non-equivalent positions of protons, H1–H4, using quantum mechanical calculations. Atomic coordinates for H1–H4 in Churakov and Wunder (2004) are approximately H1: (0.88, 0.33, 0.34), H2: (0.06, 0.22, 0.15), H3: (0.07, 0.17, 0.07), and H4: (0.99, 0.27, 0.32). However, these atomic coordinates are unmatched to any sites in Northrup's model. These atomic coordinates might be reconciled to H1: (0.62, 0.33, 0.34), H2: (0.44, 0.22, 0.15), H3: (0.43, 0.17, 0.07), and H4: (0.51, 0.27, 0.32) by replacing (x, y, z) with (1/2 – x, y, z). Among them, H3 and H4 in Churakov's model correspond to H1 and H2 in Northrup's

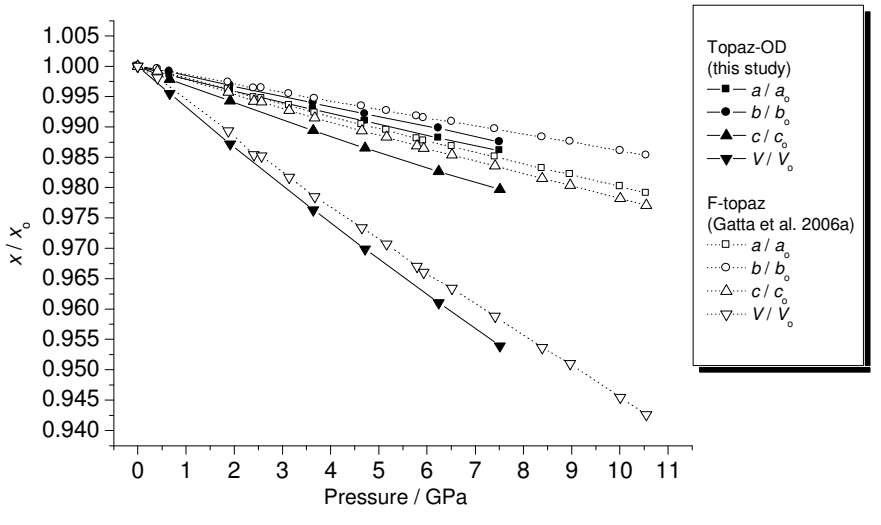

FIGURE 3. Normalized lattice parameters and unit-cell volume under pressures for topaz-OD as filled symbols (this study) and F-rich topaz as open symbols (Gatta et al. 2006a). For topaz-OD, the lattice constants and unit-cell volume are normalized to the values obtained at 7 tons instead of those in the V-can.

TABLE 2. Conditions of neutron diffraction measurements and crystallographic data for topaz-OD

Name	topaz-OD							
Chemical composition	$Al_2SiO_4(OD)_2$							
Z	4							
Load (tons)	–	7*	15	25	38	46	58	70
Pressure† (GPa)	0.0001	0.0001	0.7	1.9	3.6	4.7	6.2	7.5
Molecular weight, M_r	182.04							
Crystal system	orthorhombic							
Space group	*Pbnm* (no. 62)							
diffractometer	PEARL/HiPR at ISIS, RAL							
Specimen condition	powder in V-can	powder in Paris-Edinburgh cell						
2θ of detector bank (°)	90							
Lattice constants (Å)								
a	4.7279(2)	4.7316(6)	4.7248(3)	4.7129(3)	4.6978(3)	4.6888(4)	4.6755(5)	4.6658(4)
b	8.9269(4)	8.9328(15)	8.9250(6)	8.9046(7)	8.8786(8)	8.8624(9)	8.8410(11)	8.8210(9)
c	8.4214(4)	8.4286(13)	8.4100(5)	8.3802(6)	8.3390(6)	8.3147(7)	8.2823(9)	8.2573(7)
Unit-cell volume, V_c (Å)	355.43(3)	356.25(7)	354.64(4)	351.69(4)	347.82(4)	345.51(5)	342.36(7)	339.85(5)
Molar volume (calc.), V_m (cm³/mol)	53.51	53.63	53.39	52.95	52.37	52.02	51.54	51.16
Density (calc.), *d* (g/cm³)	3.40	3.39	3.41	3.44	3.48	3.50	3.53	3.56
d_{min} (Å)	0.5	0.55	0.55	0.55	0.55	0.55	0.55	0.55
d_{max} (Å)	4	3.5	3.5	3.5	3.5	3.5	3.5	3.5
No. data points	2079	1850	1850	1850	1835	1835	1835	1850
No. reflections	1657	1311	1353	1296	1332	1299	1319	1309
No. variables	44	19	52	52	52	52	52	52
R_P‡	0.0222	0.0489	0.0187	0.0221	0.0228	0.0278	0.0326	0.0254
R_{wp}‡	0.0199	0.0378	0.0155	0.0173	0.0180	0.0211	0.0252	0.0198
R_{F^2}‡	0.0890	0.1845	0.0924	0.0935	0.0972	0.1132	0.1198	0.1176
R_e‡	0.0166	0.0321	0.0115	0.0136	0.0146	0.0175	0.0209	0.0163
S‡	1.198	1.176	1.352	1.271	1.235	1.204	1.206	1.216

* The 7 tons data were used for determining lattice constants at 0.0001 GPa with the sample in the pressure-cell. Therefore, atomic coordinates, isotropic atomic displacement parameters, and site occupancies were fixed to the respective values refined at ambient pressure in V-can.
† Pressure was determined using the bulk modulus [K = 145(4) GPa, K' = 4; Chen and Lager 2005] with the refined unit-cell volume at respective loads as V. Also, V_o was used the refined unit-cell volume at 7 tons.
‡ The definitions of reliability indices (R_P, R_{wp}, R_{F^2}, and R_e) and goodness-of-fit (S) are shown in the footnotes of Table 1.

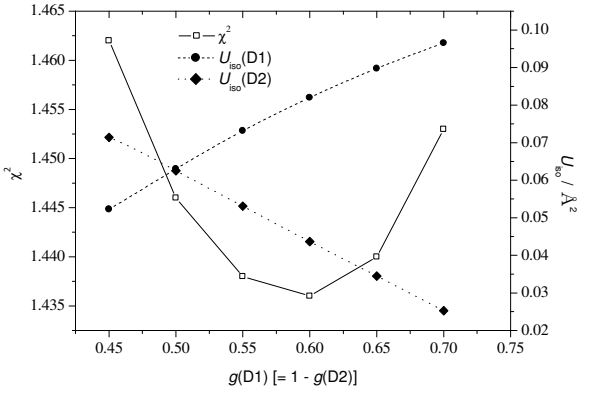

FIGURE 4. Reduced χ^2 and U_{iso} vs. g(D1) for topaz-OD at 0.0001 GPa.

TABLE 3. Structure parameters for topaz-(OD,OH) at 0.0001 GPa

Atom	site	*g*	*x/a*	*y/b*	*z/c*	$U_{iso} \times 100$ Å²
Al	8d	1	0.9062(4)	0.13273(15)	0.0797(2)	0.53(2)
Si	4c	1	0.4020(4)	0.94072(19)	0.25	0.155(18)
O1	4c	1	0.7098(3)	0.02717(15)	0.25	0.350(6)
O2	4c	1	0.4446(3)	0.75694(17)	0.25	0.350(6)
O3	8d	1	0.21408(18)	0.99286(9)	0.09325(12)	0.350(6)
O4	8d	1	0.58996(19)	0.25057(13)	0.06533(10)	0.359(6)
D1	8d	0.432(5)	0.4403(17)	0.1937(7)	0.1222(9)	7.44*
D2	8d	0.296(5)	0.556(3)	0.2978(11)	0.1720(12)	6.53*
H1†	8d	0.141(5)	0.4403(17)	0.1937(7)	0.1222(9)	7.44*
H2†	8d	0.131(5)	0.556(3)	0.2978(11)	0.1720(12)	6.53*

* The estimated standard deviation of the isotropic atomic displacement parameters (U_{iso}) for hydrogen and deuterium atoms were not calculated because U_{iso} and site occupancies (g) were alternately refined due to their serious correlation. U_{iso} was fixed in the final cycle.
† Atomic coordinates and U_{iso} for H1 and H2 were constrained to the respective values for D1 and D2.

model. Their two sites are the most favorable configurations at ambient conditions. According to Churakov and Wunder (2004), the experimentally observed low-frequency band at 3526 cm^{-1} was assigned to the O4-H3 stretching mode (O4-H1 stretching mode in Northrup's model), whereas the high-frequency band at 3600 cm^{-1} was assigned to the O4-H4 stretching mode (O4-H2 stretching mode in Northrup's model). On the other hand, our neutron results showed that the D···O distances of the hydrogen bonds in topaz-OD range from 2.053(15) Å to 2.444(14) Å, as shown in Table 5. Among them, the d(D1···O3) is the shortest, which is consistent with the assignment for the OH stretching modes by Churakov and Wunder (2004) because the shorter d(D···O) generally causes the lower stretching frequency, at least at ambient pressure. Given that the lower-frequency and higher-frequency bands are assigned to O4-H1 and O4-H2 stretching modes in Northrup's model, occupancy ratio is provided using an appropriate equation for calibration of IR band intensities to OH concentration. Thus, the corresponding ratio of site occupancies, g(H1):g(H2), was 56:44 using the equation of Libowitzky and Rossman (1997) or 58:42 using that of Paterson (1982), assuming the orientation factor, γ, is 1/3 in Paterson's equation. Hence, the IR band intensities support our neutron results showing that the occupancy [g(H1) + g(D1)] is larger than [g(H2) + g(D2)].

Hydrogen bonds in topaz-OD

The H/D positions found and illustrated in Figure 5 are in agreement with those reported for topaz-OH by Northrup et al. (1994) and topaz-OD by Chen et al. (2005). However, these previous studies proposed different hydrogen bonding schemes. That proposed by Northrup et al. (1994) possesses two trifurcated

TABLE 4. Structure parameters for topaz-OD at selected pressures

Atom	site	*g*	*x/a*	*y/b*	*z/c*	$U_{iso} \times 100$ Å^2
0.0001 GPa*						
Al	8d	1	0.9060(16)	0.1310(5)	0.0813(10)	0.16(10)
Si	4c	1	0.4034(19)	0.9432(9)	0.25	0.28(13)
O1	4c	1	0.7154(13)	0.0264(7)	0.25	0.49(5)
O2	4c	1	0.4450(14)	0.7572(9)	0.25	0.49(5)
O3	8d	1	0.2148(10)	0.9950(5)	0.0931(6)	0.49(5)
O4	8d	1	0.5932(9)	0.2529(7)	0.0640(5)	0.49(5)
D1	8d	0.59(2)	0.445(3)	0.1889(13)	0.1161(17)	8.1(6)
D2	8d	0.41(2)	0.545(3)	0.2954(15)	0.1714(17)	4.5(6)
0.7 GPa						
Al	8d	1	0.904(2)	0.1347(9)	0.0830(17)	1.11(13)
Si	4c	1	0.4006(16)	0.9401(9)	0.25	1.11(13)
O1	4c	1	0.7102(15)	0.0288(9)	0.25	0.46(5)
O2	4c	1	0.4440(17)	0.7580(9)	0.25	0.46(5)
O3	8d	1	0.2128(11)	0.9927(6)	0.0918(7)	0.46(5)
O4	8d	1	0.5948(11)	0.2506(8)	0.0637(6)	0.46(5)
D1	8d	0.59†	0.457(3)	0.1870(15)	0.1211(18)	6.0(5)
D2	8d	0.41†	0.520(4)	0.283(3)	0.1687(16)	4.7(6)
1.9 GPa						
Al	8d	1	0.902(2)	0.1340(10)	0.0843(19)	0.76(13)
Si	4c	1	0.4035(18)	0.9417(10)	0.25	0.76(13)
O1	4c	1	0.7136(17)	0.0288(10)	0.25	0.60(6)
O2	4c	1	0.443(2)	0.7580(10)	0.25	0.60(6)
O3	8d	1	0.2150(13)	0.9927(7)	0.0920(8)	0.60(6)
O4	8d	1	0.5930(12)	0.2533(9)	0.0662(7)	0.60(6)
D1	8d	0.59†	0.457(3)	0.1879(15)	0.1209(20)	6.1(6)
D2	8d	0.41†	0.526(4)	0.285(3)	0.1718(15)	4.1(6)
3.6 GPa						
Al	8d	1	0.904(3)	0.1341(10)	0.090(2)	0.78(14)
Si	4c	1	0.3978(18)	0.9412(10)	0.25	0.78(14)
O1	4c	1	0.7107(18)	0.0279(11)	0.25	0.62(6)
O2	4c	1	0.442(2)	0.7573(10)	0.25	0.62(6)
O3	8d	1	0.2151(13)	0.9930(7)	0.0896(8)	0.62(6)
O4	8d	1	0.5945(13)	0.2540(9)	0.0676(8)	0.62(6)
D1	8d	0.59†	0.464(3)	0.1846(14)	0.1215(19)	5.3(6)
D2	8d	0.41†	0.526(4)	0.278(3)	0.1756(14)	4.2(6)
4.7 GPa						
Al	8d	1	0.904(3)	0.1338(12)	0.090(3)	1.05(17)
Si	4c	1	0.402(2)	0.9418(12)	0.25	1.05(17)
O1	4c	1	0.712(2)	0.0282(12)	0.25	0.67(8)
O2	4c	1	0.445(3)	0.7584(12)	0.25	0.67(8)
O3	8d	1	0.2175(16)	0.9946(9)	0.0907(10)	0.67(8)
O4	8d	1	0.5922(15)	0.2546(11)	0.0705(10)	0.67(8)
D1	8d	0.59†	0.462(4)	0.1822(18)	0.119(3)	6.4(8)
D2	8d	0.41†	0.516(5)	0.274(4)	0.1772(17)	4.8(8)
6.2 GPa						
Al	8d	1	0.901(3)	0.1325(13)	0.090(3)	0.90(20)
Si	4c	1	0.405(3)	0.9397(14)	0.25	0.90(20)
O1	4c	1	0.718(3)	0.0251(16)	0.25	0.95(10)
O2	4c	1	0.443(3)	0.7549(14)	0.25	0.95(10)
O3	8d	1	0.2140(19)	0.9932(11)	0.0933(12)	0.95(10)
O4	8d	1	0.593(2)	0.2543(14)	0.0708(12)	0.95(10)
D1	8d	0.59†	0.467(4)	0.180(2)	0.124(3)	6.6(9)
D2	8d	0.41†	0.510(6)	0.272(5)	0.178(2)	4.6(9)
7.5 GPa						
Al	8d	1	0.906(3)	0.1316(11)	0.088(3)	1.33(17)
Si	4c	1	0.404(2)	0.9415(12)	0.25	1.33(17)
O1	4c	1	0.718(2)	0.0268(13)	0.25	1.01(8)
O2	4c	1	0.443(3)	0.7570(12)	0.25	1.01(8)
O3	8d	1	0.2193(17)	0.9967(10)	0.0913(10)	1.01(8)
O4	8d	1	0.5934(16)	0.2538(12)	0.0710(10)	1.01(8)
D1	8d	0.59†	0.456(4)	0.1808(19)	0.117(3)	7.8(8)
D2	8d	0.41†	0.519(5)	0.274(4)	0.1800(15)	3.7(6)

* The data at 0.0001 GPa were obtained from powder in a V-can. The other data at high pressures were obtained from powder in Paris-Edinburgh cell.
† The occupancies of D1 and D2 at high pressure are fixed to the values at 0.0001 GPa.

hydrogen bonds involving the H1 site, O4-H1···O2, O4-H1···O3, and O4-H1···O4", and the H2 site, O4'-H2···O1', O4'-H2···O2', and O4'-H2···O4. The labels of the oxygen sites correspond to those shown in Figure 5a (see also Fig. 2 in Northrup et al. 1994). Chen et al. (2005) proposed the same trifurcated set of contacts involving the D1 site but suggested a different bonding configuration for the D2 site, namely, O4'-D2···O1', O4'-D2···O2, and O4'-D2···O4 (see also Fig. 3 in Chen et al. 2005). We propose a different hydrogen bonding arrangement, composed of a bifurcated hydrogen bond involving the D1 site, O4-D1···O2, and O4-D1···O3 and a trifurcated hydrogen bond involving the D2 site, O4'-D2···O1, O4'-D2···O2, and O4'-D2···O4, shown as broken lines in Figure 5a.

There are at least two strands of evidence based on our data that support this hydrogen-bonding scheme. First, the *d*(D···O) contact distances of O4'-D2···O1' and O4'-D2···O2' all exceed 2.5 Å and the O-D-O angles of these motifs are less than 90° (Fig. 5b). Hence, these pairs could be excluded as candidates of hydrogen bond donor and acceptor pairs. In the more arguable case of O4-D1···O4" and O4-D1···O1', the interaction of two other more likely candidates (O4-D1···O2 and O4-D1···O3) will dominate the former after a comparison the relevant contact distances and angles (Fig. 5b).

Second, on geometrical grounds, the D1 site lies within a triangle consisting of O4, O2, and O3, shown as the pink shade in Figure 5a, and the D2 site lies in the deformed tetrahedron consisting of O4', O1, O2, and O4. Thus, the hydrogen bond involving the D1 and D2 sites should really be considered as bifurcated and trifurcated hydrogen bonding interactions.

Hydrogen bond geometry under pressure

Based on the proposed hydrogen bonding scheme for topaz-OD, Figures 6a, 6b, and 6c show the geometrical parameters *d*(O···O), *d*(D···O), and O-D-O angle, respectively, as a function of pressure. All of the *d*(O···O) contacts show a decreasing trend with increasing pressure (Fig. 6a). However, Figures 6b and 6c show that *d*(D1···O2) and *d*(D2···O1) increase or remain almost constant with increasing pressure, while the corresponding hydrogen bond angles, O4-D1-O2 and O4-D2-O1 decrease with pressure (Fig. 6c). The other D···O distances [*d*(D1···O3), *d*(D2···O2), and *d*(D2···O4)] all decrease with pressure, while the corresponding angles, O4-D1-O3, O4-D2-O2, and O4-D2-O4 all increase with pressure.

It is generally accepted that a shortening of *d*(D···O) and a straightening of O-D-O angle corresponds to a strengthening of the hydrogen bonding interaction between each donor and acceptor pair, and vice versa. Thus, the observed pressure responses for hydrogen bonding geometry used here suggests that the donor-acceptor pair interaction strengthens for O4-D1···O3, O4-D2···O2, and O4-D2···O4, and weakens for O4-D1···O2 and O4-D2···O1 with increasing pressure. Similarly, these results are again apparent from the perspective of the acceptor capability of acceptor oxygen. hydrogen bonding interaction is governed by the donor strength and the acceptor capability as described above. The acceptor capability of O3 and O4 atoms, which are the acceptor oxygen of the strengthened interaction of donor-

TABLE 5. Selected geometric parameters for topaz-OD

Pressure (GPa)	0.0001	0.7	1.9	3.6	4.7	6.2	7.5
Al octahedron							
Al-O1 (Å)	1.924(9)	1.925(13)	1.895(15)	1.87(2)	1.86(2)	1.84(2)	1.85(2)
Al-O2 (Å)	1.945(9)	1.924(13)	1.919(15)	1.872(15)	1.87(2)	1.86(2)	1.87(2)
Al-O3 (Å)	1.902(8)	1.934(11)	1.942(12)	1.924(12)	1.92(2)	1.91(2)	1.88(2)
Al-O3 (Å)	1.936(9)	1.938(13)	1.94(2)	1.95(2)	1.97(2)	1.96(2)	1.96(2)
Al-O4 (Å)	1.832(9)	1.839(13)	1.847(15)	1.87(2)	1.88(2)	1.89(2)	1.87(2)
Al-O4 (Å)	1.842(9)	1.797(12)	1.807(12)	1.813(13)	1.82(2)	1.81(2)	1.82(2)
Ave. Al-O (Å)	1.897	1.893	1.891	1.885	1.886	1.878	1.875
Polyhedral volume (Å^3)	9.04	8.98	8.96	8.86	8.87	8.76	8.74
λ*	1.005	1.006	1.006	1.006	1.006	1.006	1.005
σ^2* (deg.^{2})	13.97	16.09	16.29	18.02	17.70	18.84	14.05
Si tetrahedron							
Si-O1 (Å)	1.651(11)	1.663(11)	1.654(12)	1.659(12)	1.645(14)	1.64(2)	1.646(14)
Si-O2 (Å)	1.673(11)	1.638(11)	1.647(13)	1.647(13)	1.64(2)	1.64(2)	1.637(15)
Si-O3 (×2) (Å)	1.660(7)	1.667(7)	1.658(8)	1.654(8)	1.649(10)	1.646(12)	1.642(10)
Ave. Si-O (Å)	1.661	1.659	1.654	1.654	1.646	1.645	1.642
Polyhedral volume (Å^3)	2.35	2.34	2.32	2.32	2.29	2.28	2.27
λ*	1.001	1.001	1.001	1.000	1.001	1.002	1.001
σ^2* (deg.^{2})	3.89	3.36	3.32	0.74	1.90	7.04	3.48
Hydrogen bond geometry							
O4-D1 (Å)	1.01(2)	0.99(2)	0.98(2)	0.98(2)	0.97(2)	0.98(2)	0.99(2)
O4-D2 (Å)	1.007(15)	0.99(2)	0.98(2)	0.98(2)	0.97(2)	0.98(2)	0.98(2)
O4(-D1)···O2 (Å)	2.988(7)	2.990(9)	2.960(10)	2.945(8)	2.929(13)	2.91(2)	2.906(13)
O4(-D1)···O3 (Å)	2.926(7)	2.935(8)	2.933(10)	2.929(10)	2.902(12)	2.916(15)	2.867(13)
O4(-D2)···O1 (Å)	3.039(8)	3.077(9)	3.037(11)	3.011(11)	2.992(13)	2.95(2)	2.960(14)
O4(-D2)···O2 (Å) [=*d*(O4(-D1)···O2)]							
O4(-D2)···O4 (Å)	3.133(6)	3.133(7)	3.081(8)	3.042(9)	2.985(12)	2.969(14)	2.956(12)
D1···O2 (Å)	2.24(2)	2.27(2)	2.26(2)	2.28(2)	2.30(2)	2.28(2)	2.26(2)
D1···O3 (Å)	2.053(15)	2.099(15)	2.094(15)	2.082(14)	2.03(2)	2.05(2)	1.97(2)
D2···O1 (Å)	2.444(14)	2.63(2)	2.58(2)	2.62(3)	2.66(3)	2.64(4)	2.61(3)
D2···O2 (Å)	2.43(2)	2.31(2)	2.32(2)	2.29(2)	2.25(3)	2.20(3)	2.23(3)
D2···O4 (Å)	2.272(15)	2.296(15)	2.237(14)	2.176(14)	2.14(2)	2.12(2)	2.09(2)
O4-D1-O2 (°)	129.6(5)	128.3(5)	127.2(6)	124.1(6)	121.5(7)	120.8(7)	121.9(7)
O4-D1-O3 (°)	143.8(6)	141.2(6)	142.7(6)	143.9(6)	147.8(7)	146.0(8)	149.3(8)
O4-D2-O1 (°)	117.2(5)	107.6(5)	108.7(5)	104.1(5)	100.6(6)	98.5(6)	101.2(6)
O4-D2-O2 (°)	114.0(5)	124.9(6)	122.0(6)	123.3(6)	126.0(7)	127.9(7)	124.5(7)
O4-D2-O4 (°)	142.7(5)	141.2(6)	143.4(6)	146.7(7)	145.0(8)	143.3(8)	145.5(8)
Distances between opposing deuterium sites							
D1···D1 (Å)	2.26(2)	2.17(2)	2.16(2)	2.14(2)	2.18(3)	2.09(3)	2.20(4)
D1···D2 (Å)	2.08(2)	1.99(2)	1.97(2)	1.90(2)	1.90(3)	1.84(3)	1.89(3)
D2···D2 (Å)	1.32(2)	1.37(2)	1.31(2)	1.24(2)	1.21(2)	1.19(2)	1.16(2)

*λ, quadratic elongation and σ^2, bond angle variance are the parameters that described the distortion of polyhedra (Robinson et al. 1971).

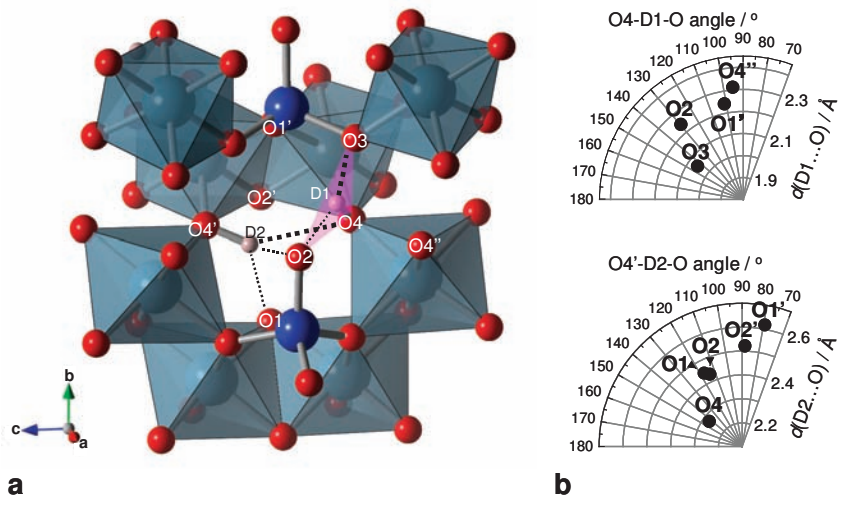

a b

FIGURE 5. (**a**) The local structure surrounding the deuterium atoms in topaz-OD. The broken lines denote the candidates for hydrogen bonds. The pink-shaded region denotes a plane consisting of O4, O2, and O3 atoms. (**b**) Polar plots of *d*(D···O) and O-D-O angles at ambient pressure for D1 (upper) and D2 (lower). The labels of each site correspond to that of (**a**). [Symmetry codes: (O1) $-1/2+x, 1/2-y, 1-z$; (O1') $1-x, 1-y, 1-z$; (O2) $1/2+x, 3/2-y, 1-z$; (O2') $-1/2+x, 3/2-y, 1-z$; (O3) $1-x, 2-y, 1/2+z$; (O4) $1-x, 1-y, 1/2+z$; (O4') $1-x, 1-y, 1-z$; (O4") $3/2-x, 1/2+y, 1/2-z$; (D1) $1-x, 1-y, 1/2+z$; (D2) $1-x, 1-y, 1-z$]. Note that color is only online version.

acceptor pairs, would increase with pressure, whereas that of O1 atom decreases with pressure.

Al octahedra under pressure

The Al site in topaz-OH or topaz-OD lies on a general position, so that the Al octahedron has six distinct Al-O bonds. Figure 7 depicts the formation of chains of edge-sharing Al octahedra and corner-sharing Si tetrahedra, in which the polyhedral arrangement resembles that of F-rich topaz. The corresponding edge-sharing chain consisting of AlO_4F_2 octahedra parallel to **z** in F-rich topaz was called the "crankshaft-like chain" by Ribbe and Gibbs (1971).

The six *d*(Al-O) bond distances and their average are plotted as a function of pressure in Figure 8a. With increasing pressure the *d*(Al-O1) and the *d*(Al-O2) decrease while one of the two *d*(Al-O4) increases. At the same time, the two *d*(Al-O3) and another *d*(Al-O4) are almost constant or decrease slightly with pressure. Accordingly, the average *d*(Al-O), shown as the bold line in Figure 8a, decreases slightly with pressure. Since the *d*(Si-O) was restrained in the refinements, it is difficult to discuss the compression behavior of Si-O bond in the strict sense. Yet generally speaking the *d*(Si-O) are almost constant with pressure. Hence, the overall volume change of topaz-OD is dominated by the compression of Al octahedra and voids, as was also observed in the reported high-pressure studies on F-rich topaz (Komatsu et al. 2003; Gatta et al. 2006a). Figure 8b shows, however, that the *d*(Al-O) or *d*(Al-OH,F) distances in F-rich topaz all decrease monotonically or are almost constant with increasing pressure. Compared to F-rich topaz, therefore, the Al octahedral compression behavior in topaz-OD is more complex, which may be related to the varying strength of interaction between hydrogen bond donors and acceptors. As mentioned above, the *d*(Al-O1) contact distance is the most compressible of the six Al-O bonds, whereas the acceptor capability of O1 is reduced with pressure. The decreasing acceptor capability of the O1 site with pressure affects the bond valence of Al-O1 bond. On the other hand, *d*(Al-O3) and *d*(Al-O4) are constant (or slightly increase) with increasing pressure, whereas the acceptor capability of O3 and O4 atoms are increased.

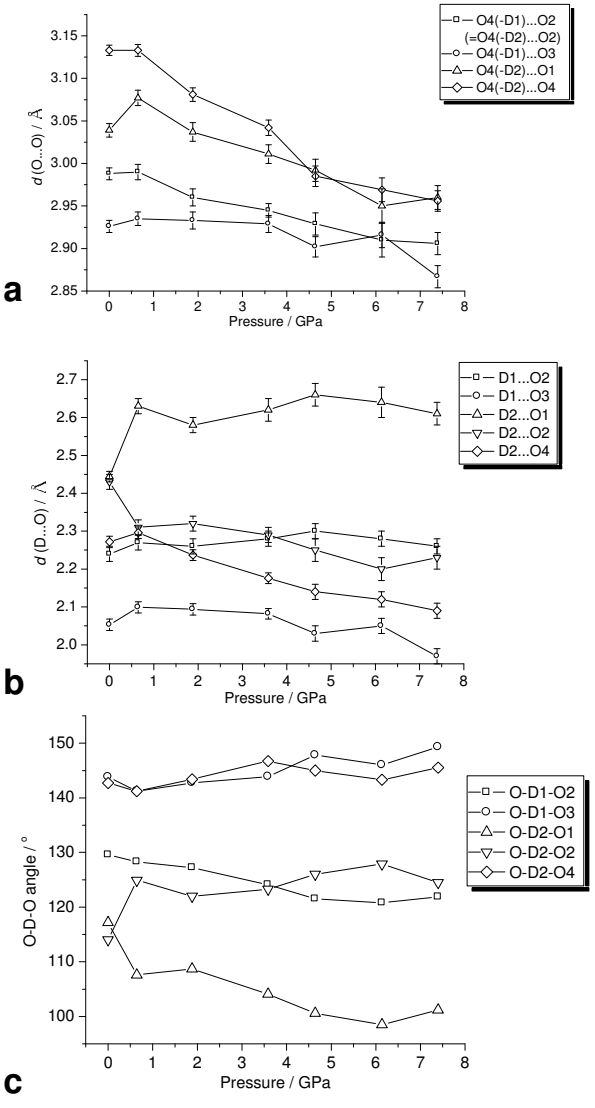

FIGURE 6. Hydrogen bonding geometrical parameters for topaz-OD as a function of pressure: (**a**) *d*(O···O), (**b**) *d*(D···O), and (**c**) the O-D-O angles of the hydrogen bonding contacts shown in Figure 5. The errors in **c** are omitted as the estimated standard deviations are smaller than the symbols.

Comparison to spectroscopic results

Here, we tacitly assume that the hydrogen bonding geometry in topaz-OD behaves identically to that in topaz-OH as a function of pressure. This is reasonable on the grounds that the geometrical isotope effect i.e., $d(O\cdots O)_D$ is larger than $d(O\cdots O)_H$ can be seen only in the $d(O\cdots O)_H$ region of about 2.44–2.64 Å (Ichikawa 1978). Thus, such isotope effect is absent in the case of the weak hydrogen bonds in topaz-OH or topaz-OD. As described above, topaz-OD contains the bifurcated hydrogen bond involving D1 and the trifurcated hydrogen bond involving D2. The O4-D1···O3 interaction in the bifurcated hydrogen bond and the O4-D2···O4 and O4-D2···O2 interactions in the trifurcated hydrogen bond strengthen with increasing pressure. Moreover,

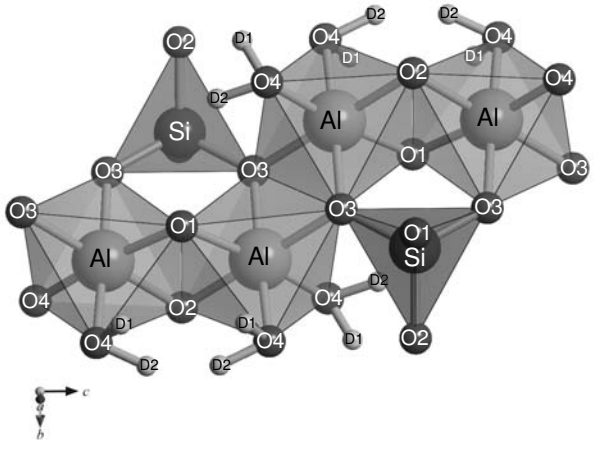

FIGURE 7. Partial structure for topaz-OD, representing the crankshaft-like chain of Al octahedra and corner-sharing Si tetrahedra.

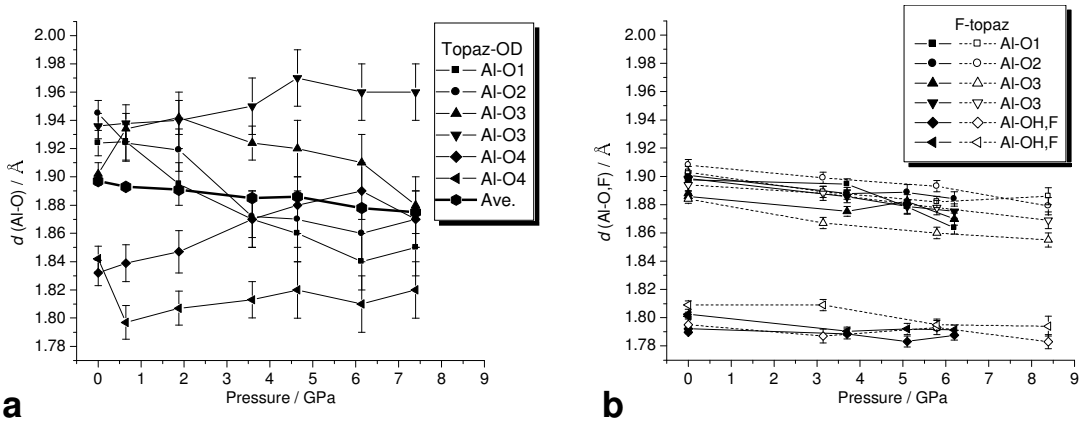

FIGURE 8. (**a**) *d*(Al-O) in topaz-OD and (**b**) *d*(Al-O,F) in F-rich topaz (filled symbols = Komatsu et al. 2003; open symbols = Gatta et al. 2006a) as a function of pressure.

the interaction strength of O4-D2···O4 is stronger than that of O4-D2···O2 because *d*(D2···O4) is shorter than *d*(D2···O2). This evolution with pressure gives rise to the so-called cooperative effect, in which the covalence of the *X*-H bonds (the hydrogen bond donor) are weakened because the donor atom *X* acts concurrently as an hydrogen bond acceptor and an hydrogen bond donor. Consequently, the acidity and donor strength of the respective hydrogen atom increases (e.g., Lutz 2003). In this case, the O4-D2···O4-D1···O3 configuration dominates the hydrogen bonding interactions of topaz-OD with increasing pressure, with the O4 atom in the O4-D1 bond being, simultaneously, an hydrogen bond donor and an acceptor. As a result of this cooperative effect, the higher the pressure, the more the donor strength is increased in the bifurcated hydrogen bond involving D1.

Additionally, *d*(Al-O3) and *d*(Al-O4) maintain their values, or slightly increase with increasing pressure. The ν(OH) is known to shift to lower wavenumbers because of the increasing *M*···OH^- distances; this was confirmed experimentally (Beckenkamp and Lutz 1992) and theoretically (Hermansson 1991). In this case, the constant or slight increasing *d*(Al-O4) gives rise to a down-shifting of ν(OH) with pressure. On the other hand, in F-rich topaz, when an OH^- ion occupies one (OH, F) site, the opposite (OH, F) site will be occupied by a fluorine atom because of H-H repulsion (e.g., Parise et al. 1980). Hence it seems likely that the cooperative effect will be absent in F-rich topaz. The absence of the cooperative effect in the case of F-rich topaz, with the decrease of all the *d*(Al-O) or *d*(Al-F) with pressure, gives rise to an increase in ν(OH).

ACKNOWLEDGMENTS

We are grateful to the ISIS facility of the CCLRC Rutherford Appleton Laboratory for the provision of neutron beam time. This experiment was performed under the Japan-U.K. Collaboration Program on Neutron Scattering. The travel costs to the U.K. for K.K. were supported by a Grant-in-Aid for Creative Scientific Research (no. 16GS0417) from the Ministry of Education, Culture, Sports, Science and Technology (MEXT) of Japan. We also thank Ronald I. Smith and Duncan J. Francis for their assistance in the POLARIS and PEARL experiments, respectively. We also thank A. Yasuda and T. Okada for help in synthesizing topaz-OD at the Earthquake Research Institute, The University of Tokyo. Figures 5 and 7 were drawn with VESTA (Momma and Izumi 2006), built into the VENUS package developed by R.A. Dilanian and F. Izumi. This work was also supported by MEXT via a Grant-in-Aid for Fellows of the Japan Society for the Promotion of Science (JSPS) no. 4681 (2005), and by a Grant-in-Aid under the 21st Century Center for Excellence (COE) program of the Advanced Science and Technology Center for the Dynamic Earth, and the Frontiers in Fundamental Chemistry program of MEXT. H.K. is grateful for a Grant-in-Aid for Scientific Research (15340190, 18654098, 18340177) from JSPS, Sumitomo Foundation and Inamori Foundation. J.B.P. is grateful for the support of the NSF through grant EAR-0510501.

REFERENCES CITED

Alberico, A., Ferrando, S., Ivaldi, G., and Ferraris, G. (2003) X-ray single-crystal structure refinement of an OH-rich topaz from Sulu UHP terrane (Eastern China)—Structural foundation of the correlation between cell parameters and fluorine content. European Journal of Mineralogy, 15, 875–881.

Beckenkamp, K. and Lutz, H.D. (1992) Lattice vibration spectra Part LXXII. OH stretching frequencies of solid hydroxides—correlation with structural and bonding data. Journal of Molecular Structure, 270, 393–405.

Besson, J.M., Nelmes, R.J., Hamel, G., Loveday, J.S., Weill, G., and Hull, S. (1992) Neutron powder diffraction above 10 GPa. Physica B, 180–181, 907–910.

Bradbury, S.E. and Williams, Q. (2003) Contrasting bonding behavior of two hydroxyl-bearing metamorphic minerals under pressure: Clinozoisite and topaz. American Mineralogist, 88, 1460–1470.

Chen, J. and Lager, G.A. (2005) High-pressure infrared and powder X-ray study of topaz-OH: Comparison with hydrous magnesium silicate (humite). COMPRES 4th annual meeting, Mohonk Mountain House, New Paltz, New York, 16–19 June 2005.

Chen, J., Lager, G.A., Kunz, M., Hansen, T.C., and Ulmer, P. (2005) A Rietveld refinement using neutron powder diffraction data of a fully deuterated topaz, $Al_2SiO_4(OD)_2$. Acta Crystallographica, E61, i253–i255.

Churakov, S.V. and Wunder, B. (2004) Ab-initio calculations of the proton location in topaz-OH, $Al_2SiO_4(OH)_2$. Physics and Chemistry of Minerals, 31, 131–141.

Eckert, H., Yesinowski, J.P., Silver, L.A., and Stolper, E.M. (1988) Water in silicate glasses: Quantification and structural studies by ^{1}H solid echo and MAS-NMR methods. Journal of Physical Chemistry, 92, 2055–2064.

Emsley, J. (1980) Very strong hydrogen bonding. Chemical Society Reviews, 9, 91–124.

Friedrich, A., Lager, G.A., Ulmer, P., Kunz, M., and Marshall, W.G. (2002) High-pressure single-crystal X-ray and powder neutron study of F, OH/OD-chondrodite: Compressibility, structure, and hydrogen bonding. American Mineralogist, 87, 931–939.

Gatta, G.D., Nestola, F., and Boffa-Ballaran, T. (2006a) Elastic behavior and structural evolution of topaz at high pressure. Physics and Chemistry of Minerals, 33, 235–242.

Gatta, G.D., Nestola, F., Bromiley, G.D., and Loose, A. (2006b) New insight into crystal chemistry of topaz: A multi-methodological study. American Mineralogist, 91, 1839–1846.

Grevel, K.-D., Fasshauer, D.W., and Rohling, S. (2000) Bulk moduli and *P-V-T* data of the high-pressure phases topaz-OH, $Al_2SiO_4(OH)_2$, and phase Pi, $Al_3Si_2O_7(OH)_3$. Journal of Conference Abstracts, 5, 1, EMPG VIII, Eighth International Symposium on Experimental Mineralogy, Petrology and Geochemistry, Abstracts.

Hermansson, K. (1991) Ab initio calculations of the fundamental OH frequency of bound OH-ions. Journal of Chemical Physics, 95, 3578–3588.

Hofmeister, A.M., Cynn, H., Burnley, P.C., and Meade, C. (1999) Vibrational spectra of dense, hydrous magnesium silicates at high pressure: Importance of the hydrogen bond angle. American Mineralogist, 84, 454–464.

Ichikawa, M. (1978) The O-H vs. O···O distance correlation, the geometric isotope effect in OHO bonds, and its application to symmetric bonds. Acta Crystallographica, B34, 2074–2080.

Jackson, R.A. and Valerio, M.E.G., (2004) A computational study of the structure, lattice and defect properties of pure and doped F^- and OH^- topaz. Journal of Physics: Condensed Matter, 16, S2771–S2779.

Jeffrey, G.A. (1997) An introduction to hydrogen bonding. Oxford University Press, U.K.

Joubert, J.-M., Černý, R., Latroche, M., Percheron-Guégan, A., and Yvon, K. (1998) Site occupancies in the battery electrode material $LaNi_{3.55}Mn_{0.4}Al_{0.3}Co_{0.75}$ as determined by multiwavelength synchrotron powder diffraction. Journal of Applied Crystallography, 31, 327–332.

Kagi, H., Nagai, T., Loveday, J.S., Wada, C., and Parise, J.B. (2003) Pressure-induced phase transformation of kalicinite ($KHCO_3$) at 2.8 GPa and local structural changes around hydrogen atoms. American Mineralogist, 88, 1446–1451.

Komatsu, K., Kagi, H., Kuribayashi, T., Parise, J.B., and Kudoh, Y. (2005) Pressure dependence of the OH-stretching mode in F-rich natural topaz and topaz-OH. American Mineralogist, 90, 266–270.

Komatsu, K., Kuribayashi, T., and Kudoh, Y. (2003) Effect of temperature and pressure on the crystal structure of topaz, $Al_2SiO_4(OH, F)_2$. Journal of Mineralogical and Petrological Sciences, 98, 167–180.

Larson, A.C. and Von Dreele, R.B. (1994) General structure analysis system (GSAS). Los Alamos National Laboratory Report LAUR 86–748.

Libowitzky, E. (1999) Correlation of O-H stretching frequencies and O-H···O hydrogen bond lengths in minerals. Monatshefte für Chemie/Chemical Monthly, 130, 1047–1059.

Libowitzky, E. and Rossman, G.R. (1997) An IR calibration for water in minerals. American Mineralogist, 82, 1111–1115.

Lutz, H.D. (1988) Bonding and structure of water molecules in solid hydrates. Correlation of spectroscopic and structural data. Structure and Bonding (Berlin), 69, 97–125.

——— (2003) Structure and strength of hydrogen bonds in inorganic solids. Journal of Molecular Structure, 646, 227–236.

Lutz, H.D., Beckenkamp, K., and Möller, H. (1994) Weak hydrogen bonds in solid hydroxides and hydrates. Journal of Molecular Structure, 322, 263–266

Marshall, W.G. and Francis, D.J. (2002) Attainment of near-hydrostatic compression conditions using the Paris-Edinburgh cell. Journal of Applied Crystallography, 35, 122–125.

Mikenda, W. (1986) Stretching frequency versus bond distance correlation of O-D(H)···Y (Y = N, O, S, Se, Cl, Br, I) hydrogen bonds in solid hydrates. Journal of Molecular Structure, 147, 1–15.

Momma, K. and Izumi, F. (2006) An integrated three-dimensional visualization system, VESTA, using wxWidgets. Commission on Crystallographic Computing, IUCr Newsletter, 7, 106–119.

Nakamoto, K., Margoshes, M., and Rundle, R.E. (1955) Stretching frequencies as a function of distances in hydrogen bonds. Journal of American Chemical Society, 77, 6480–6486.

Northrup, P.A., Leinenweber, K., and Parise, J.B. (1994) The location of H in the high-pressure synthetic $Al_2SiO_4(OH)_2$ topaz analogue. American Mineralogist, 79, 401–404.

Novak, A. (1974) Hydrogen bonding in solids: Correlation of spectroscopic and crystallographic data. Structure and Bonding (Berlin), 18, 177–216.

Parise, J.B., Cuff, C., and Moore, F.H. (1980) A neutron diffraction study of topaz: evidence for lower symmetry. Mineralogical Magazine, 43, 943–944.

Paterson, M.S. (1982) The determination of hydroxyl by infrared absorption in quartz, silicate glasses and similar materials. Bulletin de Minéralogie, 105, 20–29.

Pinheiro, M.V.B., Fantini, C., Krambrock, K., Persiano, A.I.C., Dantas, M.S.S., and Pimenta, M.A. (2002) OH/F substitution in topaz studied by Raman spectroscopy. Physical Review, B65, 104301.

Ribbe, P.H. and Gibbs, G.V. (1971) The crystal structure of topaz and its relation to physical properties. American Mineralogist, 56, 24–30.

Ribbe, P.H. and Rosenberg, P.E. (1971) Optical and X-ray determinative methods for fluorine in topaz. American Mineralogist, 57, 168–187.

Robinson, K., Gibbs, G.V., and Ribbe, P.H. (1971) Quadratic elongation: A quantitative measure of distortion in coordination polyhedra. Science, 172, 3983, 567–570.

Wunder, B., Andrut, M., and Wirth, R. (1999) High-pressure synthesis and properties of OH-rich topaz. European Journal of Mineralogy, 11, 803–813.

Wunder, B., Rubie, D.C., Ross, C.R. II, Medenbach, O., Seifert, F., and Schreyer, W. (1993) Synthesis, stability, and properties of $Al_2SiO_4(OH)_2$: A fully hydrated analogue of topaz. American Mineralogist, 78, 285–297.

Xue, X. and Kanzaki, M. (2004) Dissolution mechanisms of water in depolymerized silicate melts: Constraints from ^1H and ^{29}Si NMR spectroscopy and ab initio calculations. Geochimica et Cosmochimica Acta, 68, 5027–5057.

Manuscript received October 19, 2006
Manuscript accepted September 12, 2007
Manuscript handled by G. Diego Gatta